DK-1754-5

PPPL-2333 PPPL-2333

UC20-F

156
6/5/86

PPPL--2333

DE86 011172

ASSESSMENT OF EDDY CURRENT EFFECTS ON COMPRESSION EXPERIMENTS IN THE TFTR TOKAMAK

By

K.L. Wong and W. Park

MAY 1986

PLASMA PHYSICS LABORATORY

PRINCETON UNIVERSITY
PRINCETON, NEW JERSEY

PREPARED FOR THE U.S. DEPARTMENT OF ENERGY,
UNDER CONTRACT DE-AC02-76-CHO-3073.

Printed in the United States of America

Available from:

National Technical Information Service
U.S. Department of Commerce
5285 Port Royal Road
Springfield, Virginia 22161

Price Printed Copy $ ___*___ ; Microfiche $4.50

*Pages	NTIS Selling Price
1-25	$7.00
25-50	$8.50
51-75	$10.00
76-100	$11.50
101-125	$13.00
126-150	$14.50
151-175	$16.00
176-200	$17.50
201-225	$19.00
226-250	$20.50
251-275	$22.00
276-300	$23.50
301-325	$25.00
326-350	$26.50
351-375	$28.00
376-400	$29.50
401-425	$31.00
426-450	$32.50
451-475	$34.00
476-500	$35.50
500-525	$37.00
526-550	$38.50
551-575	$40.00
567-600	$41.50

For documents over 600 pages, add $1.50 for each additional 25-page increment.

ASSESSMENT OF EDDY CURRENT EFFECTS

ON COMPRESSION EXPERIMENTS IN THE TFTR TOKAMAK

MASTER

K.L. Wong and W. Park

Princeton Plasma Physics Laboratory

Princeton University, Princeton, NJ 08544

ABSTRACT

The eddy current induced on the TFTR vacuum vessel during compression experiments is estimated based on a cylindrical model. It produces an error magnetic field that generates magnetic islands at the rational magnetic surfaces. The widths of these islands are calculated and found to have some effect on electron energy confinement. However, resistive MHD simulation results indicate that the island formation process can be slowed down by plasma rotation.

I. INTRODUCTION

Plasma heating via adiabatic compression[1] has been demonstrated in a number of tokamak experiments.[2-5] Major-radius compression experiments were carried out in ATC[2] (Adiabatic Toroidal Compressor) and TFTR[4,5] (Tokamak Fusion Test Reactor). In both experiments, the central electron temperature rise was somewhat lower than expected based on adiabatic scaling ($T \rightarrow C^{4/3}\, T$ where C is the compression ratio). Preliminary transport analysis[4] of the TFTR data indicated that the electron energy confinement time dropped significantly (a factor of 2) during and immediately after compression. It should be pointed out that interpretation of experimental data may be significantly affected by sawtooth effects,[6] and the results from transport analysis are not conclusive. The cause of confinement deterioration is not known. As we know, major-radius compression is carried out by rapidly raising the vertical magnetic field. The transient eddy current induced in the surrounding conductors becomes a source of magnetic field error that may be large enough to degrade plasma confinement. The purpose of this paper is to assess this effect in the TFTR compression experiments. We place the emphasis on the qualitative features of various physical processes instead of the quantitative details. Since the vacuum vessel is the conductor closest to the plasma, the eddy current induced there plays a dominant role. Therefore, we neglect the presence of other conducting materials.

A current filament model[7] was previously used to calculate the eddy current and the associated magnetic field. This technique replaces the conducting vacuum vessel by a small number of current filaments along which the eddy current flows. Due to the highly discrete nature of the filament model, the spatial variation of the magnetic field $\delta\vec{B}(\vec{r})$ produced by the eddy current is highly distorted near the filaments. We shall see later that the spatial information is essential in the assessment of magnetic field error effects. An accurate spatial dependence of $\delta\vec{B}(\vec{r})$ would require a large number of current filaments, which is impractical due to the long computation time. In Sec. II of this paper, we approximate the toroidal vacuum vessel with a cylindrical one. With such an approximation, the analysis becomes much simpler. We can analyze the eddy current induced on the vessel with solid sections segmented by ports and bellows of realistic dimensions. The eddy current can generate magnetic islands[8-12] on rational magnetic surfaces. The widths of these islands are calculated in Sec. III and the island formation time is discussed in Sec. IV.

II. EDDY CURRENT CALCULATION

The TFTR vacuum vessel consists of many 0.5-in.-thick, solid stainless steel sections joined together by Inconel bellows, which have a much higher resistance. The original design has 20 solid sections and 20 bellows. Six bellows were removed to make room for the neutral beam injectors. One bellows section is covered by stainless steel plates to prevent leakage. Therefore, only 13 bellows remain effective. There are many ports on the solid sections for vacuum pumping, neutral beam injection, and various diagnostic purposes. Two neutral beamlines were connected to the vacuum vessel from the previous run period (June 1984 - April 1985). The schematic of the TFTR vacuum vessel is shown in Fig. 1.

Let us consider a cylindrical vacuum vessel with radius r_1 the same as the torus minor radius (r_1 = 1.143 m). The lengths of the solid sections are taken to be those on the vertical midplane of the toroidal vessel. We realize that this is not a good approximation for the toroidal chamber which has low aspect ratio, nevertheless, the results should have similar qualitative features and the analysis is very much simplified. Suppose the vertical field is ramped up at a constant rate $\dot{B}\hat{y}$, and we want to calculate the eddy current induced on the cylinder as well as the magnetic field generated by the eddy current.

We can start with Ampere's law and Faraday's law:

$$\nabla \times \vec{H} = \frac{\partial \vec{D}}{\partial t} + \vec{J} \tag{1}$$

$$\nabla \times \vec{E} = - \frac{\partial \vec{B}}{\partial t} \quad . \tag{2}$$

Since B is changing slowly enough so that the free-space electromagnetic wavelength is much longer than any linear dimension in the problem, we can neglect the displacement current in Eq. (1). Then, it is straightforward to show that

$$\nabla (\nabla \cdot \vec{E}) - \nabla^2 \vec{E} = - \frac{\partial}{\partial t} (\mu_o \vec{J}) \quad .$$

In vacuum, $J = 0$, $\nabla \cdot \vec{E} = 0$, we obtain

$$\nabla^2 \vec{E} = 0 \quad . \tag{3}$$

In the TFTR experiment, the vertical field ramp-up time is 15 ms. Take this as the period of an electromagnetic wave; the skin depth in stainless steel is calculated to be 5.3 cm, which is about four times larger than the thickness of the vacuum vessel. Therefore, we can treat the vacuum vessel as a thin conducting shell with spatially dependent conductivity $\sigma(\vec{r})$. In the solid sections, σ equals the conductivity for stainless steel ($1.4 \times 10^4\ \Omega^{-1}\ cm^{-1}$);

in the bellows sections and at the ports on the solid sections, $\sigma = 0$. The current density is related to the electric field via Ohm's law:

$$\vec{J} = \sigma \vec{E} \quad . \tag{4}$$

The equilibrium field coils are located outside the vacuum vessel. They generate a vertical field $\vec{B} = B\hat{y}$ which is ramped up at a constant rate $\dot{B}$. This varying magnetic field can be replaced by the following inductive electric field:

$$\vec{E} = \dot{B}\, x\, \hat{z} = \dot{B}\, r \cos\theta\, \hat{z} \quad . \tag{5}$$

Now we have a well-defined boundary value problem: We solve Eq. (3) subjected to the boundary condition given by Eq. (5). Once we get the electric field, we can use Eq. (4) to calculate the eddy current and the magnetic field associated with it. Unfortunately, the solution of such a problem is not simple. We carry this a few steps further in the appendix to show that the solution is too complicated for our purpose. Therefore, we have to look for a simpler method to estimate the eddy current. With some physical insight, we can write the electric field in the following form:

$$\vec{E} = \dot{B}\, r \cos\theta\, \hat{z} - \nabla \psi \quad . \tag{6}$$

The first term gives the ramping vertical field. It is the driving term for the eddy current. The second term represents the response due to irregular boundaries. From Ohm's law, we obtain

$$J_\theta = \sigma E_\theta \tag{7}$$

$$J_z = \sigma E_z \quad . \tag{8}$$

We assume that there is no charge accumulation on the vacuum vessel so that

$$\frac{\partial J_\theta}{\partial \theta} + \frac{\partial}{\partial z} (r \; J_z) = 0 \quad . \tag{9}$$

From Eqs. (6) to (9), we can solve for $\vec{E}$, J_θ, J_z, and ψ. The current density on the vacuum vessel is

$$J_z = \sigma \dot{B} r_1 \cos\theta + \dot{B} r_1 \frac{\partial \sigma}{\partial \theta} \sin\theta \tag{10}$$

$$J_\theta = -r_1^2 \dot{B} \frac{\partial \sigma}{\partial z} \sin\theta \quad . \tag{11}$$

Then the magnetic field can be calculated from the Biot-Savart law. The eddy current pattern is shown in Fig. 2 for a single solid section. It is apparent that the "saddle" current has a tendency to oppose the increasing vertical field change, as one would expect from Lenz's law. The magnetic field at $\vec{r}_o$ = (x_o, y_o, z_o) generated by the eddy current on one solid section of length $z_2 - z_1$ is expressed in Cartesian coordinates as follows:

$$\delta B_x = T \frac{\mu_o}{4\pi} \int_o^{2\pi} r_1 \, d\theta \int_{z_1}^{z_2} dz \frac{J_\theta \cos\theta \, (z_o - z) - J_z \, (y_o - r_1 \sin\theta)}{\rho^3} \tag{12}$$

$$\delta B_y = T \frac{\mu_o}{4\pi} \int_o^{2\pi} r_1 \, d\theta \int_{z_1}^{z_2} dz \frac{J_z \, (x_o - r_1 \cos\theta) + J_\theta \sin\theta \, (z_o - z)}{\rho^3} \tag{13}$$

$$\delta B_z = T \frac{\mu_o}{4\pi} \int_o^{2\pi} r_1 \, d\theta \int_{z_1}^{z_2} dz \, \frac{-J_\theta \sin\theta \, (y_o - r_1 \sin\theta) - J_\theta \cos\theta \, (x_o - r_1 \cos\theta)}{\rho^3} , \tag{14}$$

where

$$\rho = [a^2 + (z_o - z)^2]^{1/2}$$

$$a^2 = (x_o - r_1 \cos\theta)^2 + (y_o - r_1 \sin\theta)^2$$

T = thickness of conducting shell .

It is easy to show that the above expression of $\delta\vec{B}$ has the following symmetry properties as expected:

$$\delta B_x \, (x_o, y_o, z_o) = - \delta B_x (x_o, - y_o, z_o)$$

$$\delta B_y \, (x_o, y_o, z_o) = \delta B_y \, (x_o, - y_o, z_o)$$

$$\delta B_z \, (x_o, y_o, z_o) = - \delta B_z \, (x_o, - y_o, z_o) \quad .$$

III. MAGNETIC ISLANDS

The most undesirable effect produced by the error magnetic field $\delta\vec{B}$ is the formation of magnetic islands around each rational magnetic surface with safety factor $q = m/n$ (m and n are integers). Without the error field, let us assume that the tokamak has good circular magnetic surfaces represented by $\vec{B} = \vec{B}_\phi + \vec{B}_\theta + \vec{B}_v$, where $\vec{B}_\phi$ is the toroidal field, $\vec{B}_\theta$ is the poloidal field, and $\vec{B}_v$ is the vertical field. If we write the error field in the following form

$$\delta\vec{B} = \nabla \times (\alpha\,\vec{B}) \quad , \tag{15}$$

where

$$\alpha\,(\psi,\,\theta,\,\phi) = \sum_{n,m} \alpha_{nm}(\psi)\,\cos\,(n\phi - m\theta + \phi_{nm}) \quad , \tag{16}$$

then it can be shown[11] that the half-width of the magnetic island at radius r where $q = m/n$ is

$$\Delta r = r\,\left|\frac{4q^2}{r\,\frac{dq}{dr}}\,\frac{B_\phi}{B_\theta}\,\frac{\alpha_{nm}}{r}\right|^{1/2} \quad . \tag{17}$$

From Eq. (15), we can express the radial components of $\delta\vec{B}$ as

$$\begin{aligned} \delta B_r &= \frac{1}{r}\,[\frac{\partial}{\partial\theta}\,(\alpha\,B_\phi) - \frac{1}{R}\,\frac{\partial}{\partial\phi}\,(r\,\alpha\,B_\theta)] \\ &= \frac{B_\phi}{r}\,\frac{\partial\alpha}{\partial\theta} \quad . \end{aligned} \tag{18}$$

Therefore, α_{nm} can be obtained from the Fourier components of δB_r. This is why the spatial variation of $\delta\vec{B}$ is important. To carry out the Fourier analysis we need to integrate over two dimensions. From Eqs. (12) and (13), we see that we need to integrate over two dimensions to evaluate δB_r as well. Therefore, we have to integrate over four dimensions in order to calculate α_{nm}. This would require a very long numerical computation time. Fortunately, the z-integration in Eqs. (12) and (13) can be carried out analytically. For the solid sections without ports, $\frac{\partial\alpha}{\partial\theta} = 0$ and we get

$$\delta B_x = T \frac{\mu_o}{4\pi} r_1 \int_o^{2\pi} d\theta \left\{ \frac{r_1^2 \dot{B} \sigma \sin\theta \cos\theta (z_o - z_2)}{[a^2 + (z_o - z_2)^2]^{3/2}} - \frac{r_1^2 \dot{B} \sigma \sin\theta \cos\theta (z_o - z_1)}{[a^2 + (z_o - z_1)^2]^{3/2}} - \right.$$

$$\left. \frac{\sigma \dot{B} r_1 \cos\theta (y_o - r_1 \sin\theta)}{a^2} \left[\frac{z_2 - z_o}{[(z_2 - z_o)^2 + a^2]^{1/2}} - \frac{z_1 - z_o}{[(z_1 - z_o)^2 + a^2]^{1/2}} \right] \right\}$$

(19)

$$\delta B_y = T \frac{\mu_o}{4\pi} r_1 \int_o^{2\pi} d\theta \left\{ \frac{r_1^2 \dot{B} \sigma \sin^2\theta (z_o - z_2)}{[a^2 + (z_o - z_2)^2]^{3/2}} - \frac{r_1^2 \dot{B} \sigma \sin^2\theta (z_o - z_1)}{[a^2 + (z_o - z_1)^2]^{3/2}} \right.$$

$$\left. + \frac{\sigma \dot{B} r_1 \cos\theta (x_o - r_1 \cos\theta)}{a^2} \left[\frac{z_2 - z_o}{[a^2 + (z_2 - z_o)^2]^{1/2}} - \frac{z_1 - z_o}{[a^2 + (z_1 - z_o)^2]^{1/2}} \right] \right\}.$$

(20)

We put $\delta B_r = (\delta B_x^2 + \delta B_y^2)^{1/2}$, and its Fourier components give values for α_{nm}. It should be noted that Eq. (19) and Eq. (20) represent an error magnetic field produced by the eddy current in one solid section. When we calculate the total $\delta\vec{B}$, it is necessary to add up contributions from all the solid sections. For those sections with ports, the second term in Eq. (10) is not zero and it gives rise to an additonal term in δB_x and δB_y. In order to avoid end effects in our cylindrical model, we consider a long cylinder with three periods of length $2\pi R_o$ (R_o =2.65 m is the major radius of the toroidal chamber) and the error field is calculated in the middle period. We also tried to calculate $\delta\vec{B}$ in the middle of a five-period cylinder: the difference is less than 1%. We include four large ports in the vessel: the two pumping ports denoted by "P" and the two neutral beam ports denoted by "NB" in Fig. 1. Each port subtends a 40° poloidal angle on the large-major-radius side, and its length along the z-direction is the same as the shortest solid section. The port dimensions are chosen to be slightly different from the real ports on the vacuum vessel for computational convenience. We choose the following q-profile:

$$q(r) = 0.8 \left[1 + \frac{r^2}{r_c^2}\right]$$

with $r_c = 0.33$ meters. Then we use Eq. (17) to calculate the island widths at various rational magnetic surfaces when the plasma major radius is at R = 2.3 meters with a toroidal field $B_\phi = 3.1$ tesla. The results are listed in Table I. It should be noted that Eq. (17) is accurate only for small islands. Therefore, we double-check these results by computing δB_r on the cylindrical plasma surface, and then use it as a boundary conditon to obtain a self-consistent solution of $\nabla \times \vec{B} = \mu_o \vec{J}$ and $\nabla \cdot \vec{B} = 0$ inside the plasma. The m = 1 island computed by this method is about 30% larger than the value in Table I while the other smaller islands are the same as expected. From these results, we can see that the m = 1, n = 1 island is the largest and it can degrade the central plasma energy confinement. Sawtooth activities which appear near the q = 1 surface would mix with the externally created magnetic island. Let us assume that the region between q = 1 and q = 3 surfaces is the region of good energy confinement in the absence of an error magnetic field. With the error field, about 1/3 of the thickness of this good confinement region is occupied by the magnetic islands listed in Table I. Since heat transport across magnetic islands is a very rapid process (via electron heat conduction along magnetic field lines), the good confinement region is reduced to 2/3 of the original thickness. If energy transport across magnetic surfaces is a diffusive process, then the central energy confinement time should decrease by the factor $f = 1 - (1-1/3)^2 = 5/9$. Of course, the effect would be smaller if MHD activities like sawteeth, the $m = 2$ tearing mode, etc. exist before we impose the error magnetic field. The large $m = 1$ island can be eliminated if we compress a high-q plasma with $q(o) > 1$.

At this point, we would like to add several cautionary remarks. Although the magnetic islands tend to explain qualitatively the decrease of energy confinement time during compression, there is no direct experimental evidence of their existence. There are not enough high quality experimental data for detailed transport analysis and, therefore, the linkage between theory and experiment is tenuous at this moment. In the above calculation, we use a crude cylindrical model for the vacuum vessel and only consider the eddy current induced by the changing vertical field. These simplifications are necessary so that the analysis can be carried out with a reasonable amount of effort. During compression, the radially inward plasma motion and the increasing toroidal plasma current also induce a significant eddy current on the vacuum vessel. Its magnitude is comparable to that due to the varying vertical field and the resultant error field becomes larger. This was demonstrated in the previous calculation[7] based on a current filament model. Here we also neglect the response time of the eddy current due to the finite inductance of the current path. The results given in Table I can be taken as the value near the end of the compression stroke. The temporal evolution of the eddy current was also worked out in the filament model calculation.[7]

IV. ISLAND FORMATION TIME

Magnetic islands are formed via field line reconnection processes. The field line reconnection time can be estimated[10] by $\tau_R \sim \tau_\eta^{1/2}\, \tau_A^{1/2} = (\eta^{-1/2}$

$a_p) (a_p/V_A)^{1/2}$ where η is the plasma resistivity, a_p is the plasma minor radius and $V_A = B_\theta/(4\pi n_i m_i)^{1/2}$ is the Alfvén speed with the poloidal magnetic field B_θ. For B_ϕ = 30 kG, q equals unity at a_p = 16 cm with B_θ = 2 kG. Taking the Spitzer resistivity for T_e = 2 keV with $n_i = 3 \times 10^{13}$ cm^{-3} (D^+ ion), we get $\tau_R \sim 10^{-3}$ sec which is much shorter than the 15 ms compression time. Therefore, island formation is almost instantaneous during compression.

The islands are formed because of the broken symmetry in the vacuum vessel due to the bellows sections and the ports. It is conceivable that any realistic tokamak experiment will have an asymmetric vacuum vessel and it would be very difficult to eliminate such eddy current problems in compression experiments unless the vacuum vessel is solely designed for that purpose. Instead of optimizing the vacuum vessel geometry, we would like to consider the possibility of stretching the island formation time τ_I. The eddy current is pulsed in nature. If τ_I is much longer than the eddy current pulse, then magnetic islands will not have time to form.

One possible mechanism that may increase the island formation time is by plasma motion. In a stationary plasma, the x-points of the islands produced by the eddy current in the vacuum vessel should be stationary with respect to the vacuum vessel. When an island starts to grow via field line reconnection at the x-points, the rate of increase of magnetic flux ψ_s in the island can be described by $\dot{\psi}_s = -\eta J_s$, where J_s is the local current density at the x-point at which it is sharply peaked. As we know, tangential neutral beam injection can cause the plasma to rotate in the toroidal direction.[13] According to MHD theory, magnetic field lines are frozen in plasmas. A moving plasma will tend to drag the x-points along with it. This would make J_s broadly distributed in space, which can result in a much slower island growth rate $\dot{\psi}_s$. If the island formation time is much longer than the eddy current pulse, the topology of the magnetic flux surfaces remains unchanged and the effect of the error magnetic field on plasma energy confinement would be very small. In order to explore such a possibility, we use a resistive MHD code, IMH2D, to investigate island formation in a rotating plasma. This code has been used to study magnetic field line reconnection previously.[12] We choose a q-profile which is stable against the $m = 2$ tearing mode and then we ramp up an $m = 2$ magnetic perturbation by forcing currents through some external conductors as shown in Fig. 3. In the MHD simulation, we cannot use a realistic value for the resistivity η because it would require very small grid size and very long computational time. We choose $\eta = 10^{-4}$ ohm-cm, which is about 100 times larger than the actual value. If there is no plasma rotation, islands can form and follow the increasing magnetic perturbation closely. Figure 4a shows the $m = 2$ island computed from the MHD code. When we introduce toroidal rotation with velocity $V_\phi = 10^8$ cm/sec, we run the code up to 400 Alfvén time (τ_A), and there is still no sign of island formation. The flux surfaces are distorted as shown in Fig. 4b but their topology remains unchanged. This confirms our heuristic argument that τ_I is much longer with plasma rotation. Unfortunately, we do not know whether it is long enough for the TFTR experiment because we cannot do the MHD simulation with the actual experimental plasma parameters. We are also not certain about the scaling of τ_I with plasma parameters in rotating plasmas. This would be an interesting topic for future investigation.

ACKNOWLEDGMENTS

The authors would like to thank Professor T.H. Stix for many valuable suggestions. Discussions with M.G. Bell, A.H. Boozer, R.J. Hawryluk,

W. Stodiek, G.D. Tait, and R. White were also very helpful. This work was supported by the US Department of Energy Contract No. DE-AC02-76-CHO-3073.

APPENDIX

The electric field can be expressed in Cartesian coordinates with the axis of the cylindrical vacuum vessel as the z-axis. Equation (3) becomes

$$\nabla^2 E_{x,y,z} = 0 \quad .$$

The general solution is given in cylindrical coordinates as follows:

$$E_{x,y,z} = \sum_{m=0}^{\infty} a_m^{x,y,z} r^m e^{im\theta} + \sum_{k,m} b_{km}^{x,y,z} I_m (kr) e^{ikz + im\theta} \quad , r < r_1$$

$$E_{x,y} = \sum_{m=0}^{\infty} \frac{C_m^{x,y}}{r^m} e^{im\theta} + \sum_{k,m} d_{km}^{x,y} K_m (kr) e^{ikz + im\theta}, \; r > r_1$$

$$E_z = \dot{B} r \cos\theta + \sum_{m=0}^{\infty} \frac{C_m^z}{r^m} e^{im\theta} + \sum_{k,m} d_{km}^z K_m (kr) e^{ikz + im\theta}, \; r > r_1 \quad ,$$

where I_m and K_m are modified Bessel functions of order m. We apply Ohm's law on the thin conducting shell at $r = r_1$ and then match the inside $(r < r_1)$ and outside $(r > r_1)$ solutions on the shell to determine the coefficients $a_m^{x,y,z}$, $b_{km}^{x,y,z}$, $C_m^{x,y,z}$, $d_{km}^{x,y,z}$. For each value of m and k, there are 12 complex coefficients. Different m and k values are coupled due to the asymmetric conducting shell as well as the m = 1 driving electric field ($\dot{B} r \cos\theta$ term in E_z). Suppose we are only interested in terms with m = 1,2,3 and n = 1,2 ($k = 2\pi\, n/L$), and we only keep m ± 1, n ± 1 coupling terms. The number of coefficients to be determined is 12 (3+2) (2+2) = 240. This means that we have to work with 240 × 240 matrices, which are too complicated for our purpose.

REFERENCES

[1]H.P. Furth and S. Yoshikawa, Phys. Fluids 13, 2593 (1970).

[2]K. Bol, J.L. Cecchi, C.C. Daughney, R.A. Ellis, H.P. Eubank, et al., Phys. Rev. Lett. 32, 661 (1974).

[3]V.K. Gusev, V.A. Ipatov, M.G. Kaganskii, S.G. Kalmykov, G.T. Razdobarin, et al., JETP Lett. 22, 110 (1975).

[4]G. Tait, J. Bell, M.G. Bell, M. Bitter, W.R. Blanchard et al., Proceedings on the Tenth International Conference on Plasma Physics and Controlled Nuclear Fusion Research, (IAEA, Vienna, 1985) Vol. I, p. 141.

[5]K.L. Wong, M. Bitter, G.W. Hammett, W. Heidbrink, H. Hendel et al., Phys. Rev. Lett. 55, 2587 (1985).

[6]J. Kiraly, M. Bitter, P. Efthimion, S. von Goeler, B. Grek, et al., Princeton Plasma Physics Laboratory Report PPPL-2254, (September, 1985).

[7]J. DeLucia, M. Bell, and K.L. Wong, Princeton Plasma Physics Laboratory Report PPPL-2228, Princeton University (July, 1985).

[8]D.W. Kerst, Plasma Phys. (J. Nucl. Energy, Part C), 4, 253 (1962).

[9]M.N. Rosenbluth, R.A. Sagdeev, J.B. Taylor and G.M. Zaslavskii, Nucl. Fusion 6, 297 (1966).

[10]Alexander B. Rechester and Thomas H. Stix, Phys. Rev. Lett. 36, 587 (1976).

[11]A.H. Boozer and R.B. White, Phys. Rev. Lett. 49, 786 (1982).

[12]W. Park, D.A. Monticello, and R.B. White, Phys. Fluids 27, 137 (1984).

[13]K. Brau, M. Bitter, R.J. Goldston, D. Manos, K. McGuire, and S. Suckewer, Nucl. Fusion 23, 1643 (1983).

Table I. Magnetic island widths at various rational surfaces (r is radial location of the island)

q = m/n	r (cm)	island full width (cm)
1/1	16.4	14.9
2/1	40.1	1.24
3/1	54.3	1.14
3/2	30.6	0.19
4/2	40.1	0.27
5/2	47.7	0.26
4/3	26.7	0.14
5/3	34.1	0.13

FIGURE CAPTIONS

Fig. 1. Schematic of the TFTR vacuum vessel. P denotes pumping port and NB denotes neutral beam port

Fig. 2. Eddy current pattern in a solid section.

Fig. 3. (a) Externally imposed m = 2 magnetic perturbation.

(b) Variation of external current with time.

Fig. 4. (a) Flux plot showing m = 2 islands in a nonrotating plasma.

(b) Flux plot in a rotating plasma at $t = 400\ \tau_A$.

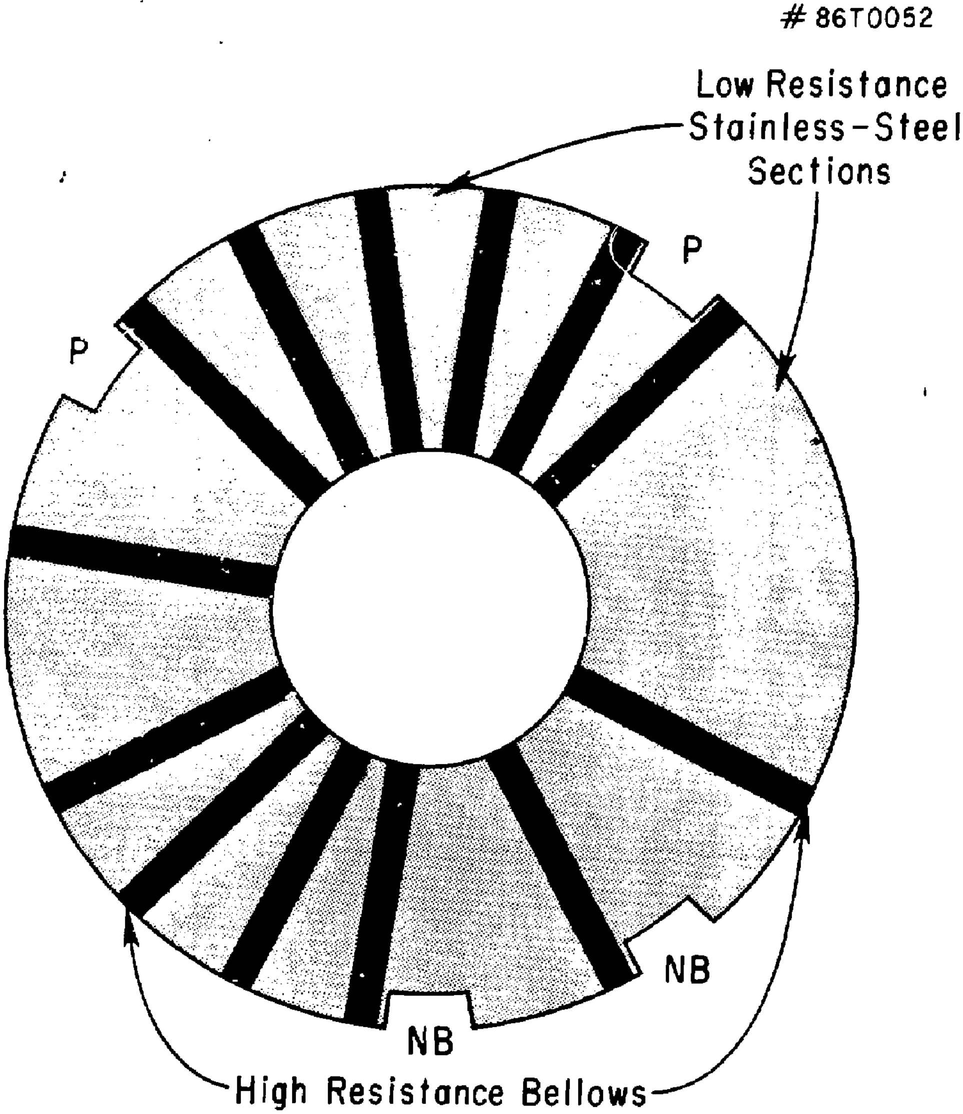

86T0052
Low Resistance Stainless-Steel Sections
P
P
NB
NB
High Resistance Bellows

Fig. 1

86X0188

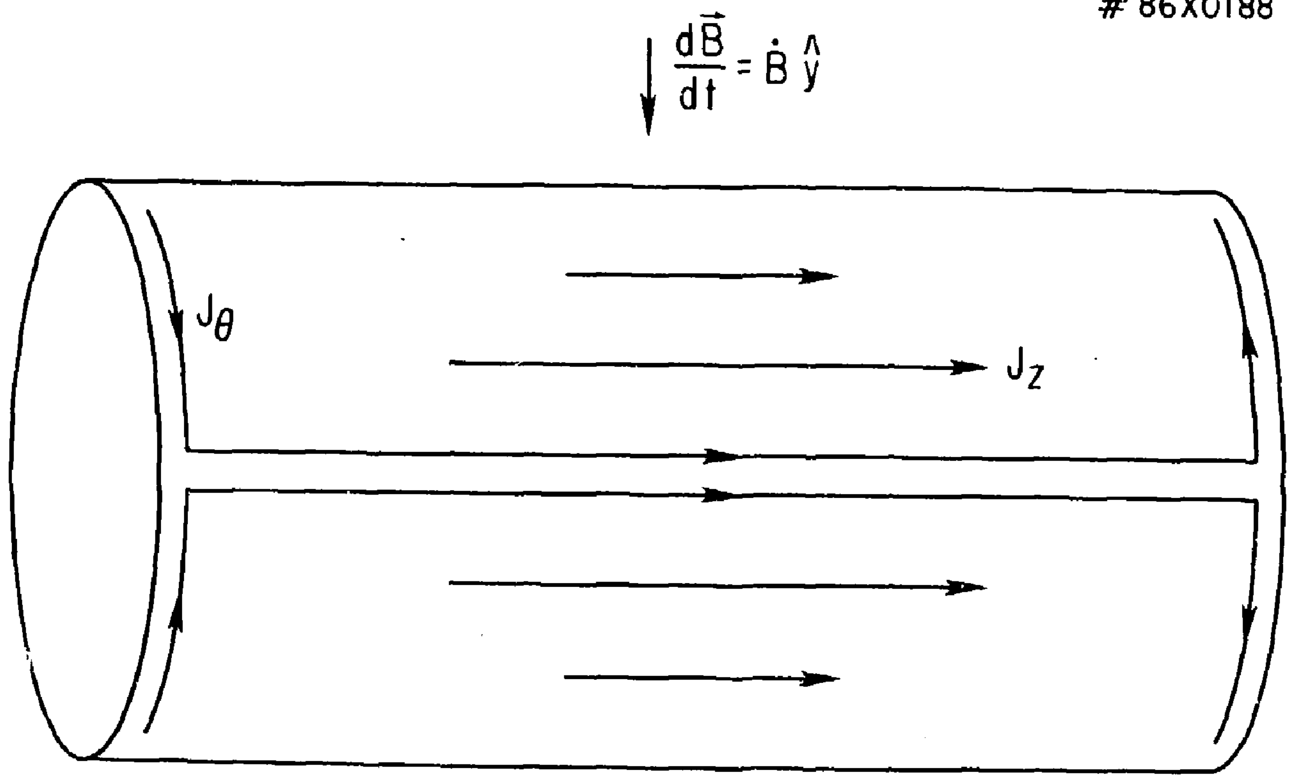

Fig. 2

#86X0186

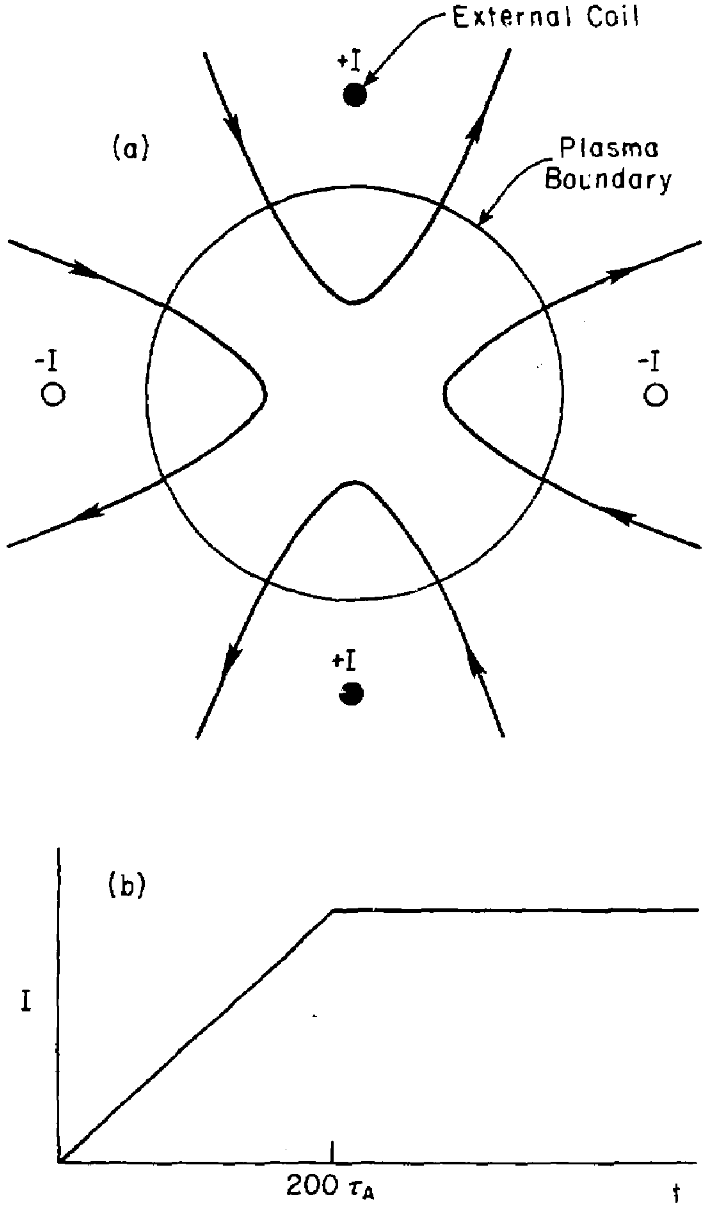

Fig. 3

#86X0187

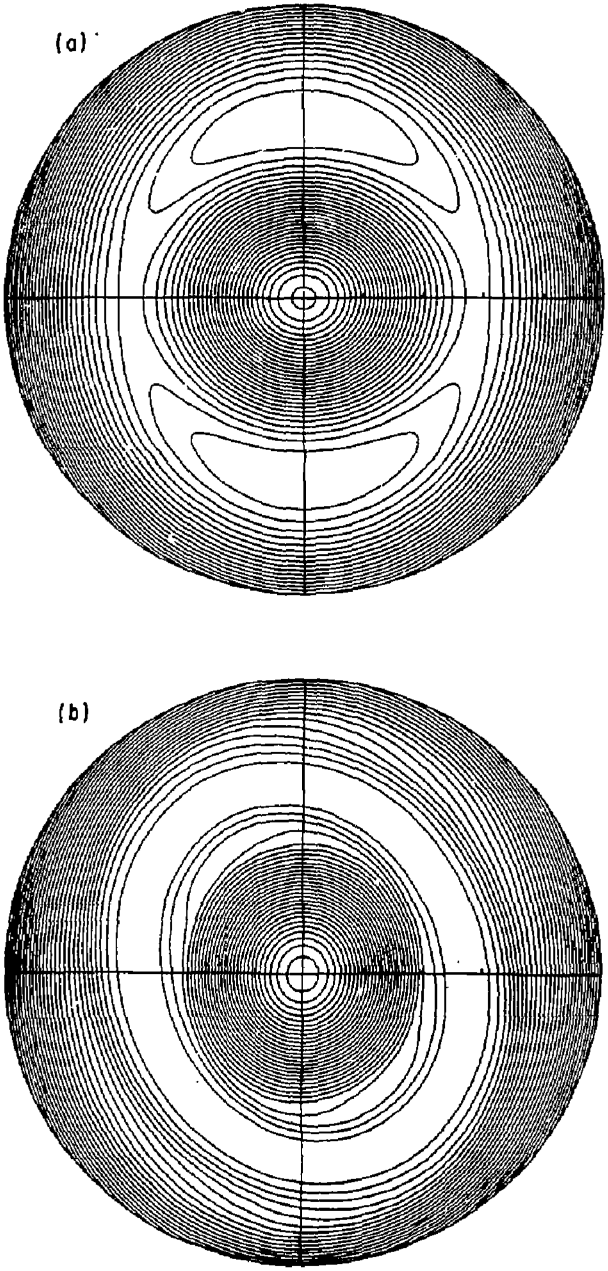

Fig. 4

EXTERNAL DISTRIBUTION IN ADDITION TO UC-20

Plasma Res Lab, Austra Nat'l Univ. AUSTRALIA
Dr. Frank J. Paoloni, Univ of Wollongong, AUSTRALIA
Prof. I.R. Jones, Flinders Univ., AUSTRALIA
Prof. M.H. Brennan, Univ Sydney, AUSTRALIA
Prof. F. Cap, Inst Theo Phys, AUSTRIA
Prof. Frank Verheest, Inst theoretische, BELGIUM
Dr. D. Palumbo, Dg XII Fusion Prog, BELGIUM
Ecole Royale Militaire, Lab de Phys Plasmas, BELGIUM
Dr. P.H. Sakanaka, Univ Estadual, BRAZIL
Dr. C.R. James, Univ of Alberta, CANADA
Prof. J. Teichmann, Univ of Montreal, CANADA
Dr. H.M. Skarsgard, Univ of Saskatchewan, CANADA
Prof. S.R. Sreenivasan, University of Calgary, CANADA
Prof. Tudor W. Johnston, INRS-Energie, CANADA
Dr. Hannes Barnard, Univ British Columbia, CANADA
Dr. M.P. Bachynski, MPB Technologies, Inc., CANADA
Chalk River, Nucl Lab, CANADA
Zhengwu Li, SW Inst Physics, CHINA
Library, Tsing Hua University, CHINA
Librarian, Institute of Physics, CHINA
Inst Plasma Phys, Academia Sinica, CHINA
Dr. Peter Lukac, Komenskeho Univ, CZECHOSLOVAKIA
The Librarian, Culham Laboratory, ENGLAND
Prof. Schatzman, Observatoire de Nice, FRANCE
J. Radet, CEN-BP6, FRANCE
AM Dupas Library, AM Dupas Library, FRANCE
Dr. Tom Mual, Academy Bibliographic, HONG KONG
Preprint Library, Cent Res Inst Phys, HUNGARY
Dr. R.K. Chhajlani, Vikram Univ. INDIA
Dr. B. Dasgupta, Saha Inst, INDIA
Dr. P. Kaw, Physical Research Lab, INDIA
Dr. Phillip Rosenau, Israel Inst Tech, ISRAEL
Prof. S. Cuperman, Tel Aviv University, ISRAEL
Prof. G. Rostagni, Univ Di Padova, ITALY
Librarian, Int'l Ctr Theo Phys, ITALY
Miss Clelia De Palo, Assoc EURATOM-ENEA, ITALY
Biblioteca, del CNR EURATOM, ITALY
Dr. H. Yamato, Toshiba Res & Dev, JAPAN
Direc. Dept. Lg. Tokamak Dev. JAERI, JAPAN
Prof. Nobuyuki Inoue, University of Tokyo, JAPAN
Research Info Center, Nagoya University, JAPAN
Prof. Kyoji Nishikawa, Univ of Hiroshima, JAPAN
Prof. Sigeru Mori, JAERI, JAPAN
Prof. S. Tanaka, Kyoto University, JAPAN
Library, Kyoto University, JAPAN
Prof. Ichiro Kawakami, Nihon Univ, JAPAN
Prof. Satoshi Itoh, Kyushu University, JAPAN
Dr. D.I. Choi, Adv. Inst Sci & Tech, KOREA
Tech Info Division, KAERI, KOREA
Bibliotheek, Fom-Inst Voor Plasma, NETHERLANDS
Prof. B.S. Liley, University of Waikato, NEW ZEALAND
Prof. J.A.C. Cabral, Inst Superior Tecn, PORTUGAL
Dr. Octavian Petrus, ALI CUZA University, ROMANIA
Prof. M.A. Hellberg, University of Natal, SO AFRICA
Dr. Johan de Villiers, Plasma Physics, Nucor, SO AFRICA
Fusion Div. Library, JEN, SPAIN
Prof. Hans Wilhelmson, Chalmers Univ Tech, SWEDEN
Dr. Lennart Stenflo, University of UMEA, SWEDEN
Library, Royal Inst Tech, SWEDEN
Centre de Recherchesen, Ecole Polytech Fed, SWITZERLAND
Dr. V.T. Tolok, Kharkov Phys Tech Ins, USSR
Dr. D.D. Ryutov, Siberian Acad Sci, USSR
Dr. G.A. Eliseev, Kurchatov Institute, USSR
Dr. V.A. Glukhikh, Inst Electro-Physical, USSR
Institute Gen. Physics, USSR
Prof. T.J.M. Boyd, Univ College N Wales, WALES
Dr. K. Schindler, Ruhr Universitat, W. GERMANY
Nuclear Res Estab, Julich Ltd, W. GERMANY
Librarian, Max-Planck Institut, W. GERMANY
Bibliothek, Inst Plasmaforschung, W. GERMANY
Prof. R.K. Janev, Inst Phys, YUGOSLAVIA